

Transport mechanism in amorphous molybdenum silicide thin films

Zhengyuan Liu, Bingcheng Luo ^{a)}, Junbiao Hu, Cheng Xing

School of Physical Science and Technology, Northwestern Polytechnical University,
Xi'an, Shaanxi, 710072, China

^{a)} Electronic mail: luobingcheng@nwpu.edu.cn

Abstract

Amorphous molybdenum silicide compounds have attracted significant interest for potential applications in optoelectronic devices, particularly in single-photon detector. In this work, the temperature-dependent electronic transport and magneto-resistance behaviors were measured to reveal the charge transport mechanism, which is of importance for applications but is still insufficient. It is found that Mott variable hopping conductivity dominated the transport of sputtered amorphous molybdenum silicide film. Additionally, a crossover from positive to negative magneto-resistance was observed, which is due to the varied probability of hopping under an applied magnetic field.

Keywords: amorphous, molybdenum silicide, magneto-resistance, variable range hopping conductivity

Introduction

Transition metal (TM) based amorphous materials have been studied in recent years due to their unique properties such as high uniformity, lower carrier density and stability of the amorphous structure [1-3]. What's more, the discovery of superconductivity in transition-metal amorphous alloys [4] further trigger general research interest. Among TM-based amorphous materials, molybdenum-based amorphous compounds have attracted a significant research due to their tunable superconducting transition temperature [5], intrinsically low flux pinning and homogeneity [6-9]. These excellent characteristics make them competitive alternatives for superconducting single photon detectors [5, 10-13]. Additionally, molybdenum-based amorphous compounds also exhibit tantalizing research interest in vortex dynamics, enabling them to optimize device performances [14]. So far, considerable efforts have been attributed to the electronic transport and magneto-transport behaviors of the molybdenum-based amorphous compounds at low temperature (below the temperature of liquid nitrogen) [7, 15-18]. By contrast, the investigation of molybdenum-based amorphous compounds is still insufficient at high temperature, but it is important for developing a comprehensive physical insight into transport behaviors and further exploring their potential applications [3]. Therefore, we here studied the electronic transport and magneto-transport behaviors of sputtered molybdenum silicide amorphous films in the relatively high temperature region (between the temperature of liquid nitrogen and room temperature). Since the electron wave function can be altered by the magnetic field, especially the localized electron

wave function, thereby the magneto-transport measurement was conducted as a powerful method to reveal the underneath transport mechanism in many crystalline and amorphous materials [19]. The extensive report about magneto-resistance (MR) in amorphous compounds dates back to 1970s in the case of Ge, Si, InSb and GeTe [20], covering many aspects such as conventional magneto-resistance, colossal magneto-resistance and giant magneto-resistance. Additionally, the negative MR and its conversion to positive MR was reported in some materials such as $\text{Ni}_x\text{Si}_{1-x}$ and $\text{Mo}_x\text{Ge}_{1-x}$ [21, 22]. In molybdenum-based amorphous compounds, however, the report of analogous MR behavior is still lacking, which is the main motivation of this work.

Experimental

Amorphous molybdenum silicide (*a*-MoSi) films with thickness of ~30 nm were deposited on silicon ($>10^5\Omega\text{ cm}$) at room temperature by radio-frequency (RF) magnetron sputtering technique. The base pressure of the chamber is less than 1×10^{-4} Pa. The RF power intensity is 2 W cm^{-1} . The sputtering pressure is 20 mTorr in pure argon ambient. Prior to deposition, the target is pre-sputtered for 30 min to eliminate the influence of target surface. A commercial atomic force microscopy (AFM) (MFP-3D, Asylum Research) was used to measure the surface topography. The film structure and chemical compositions were determined by grazing incidence X-ray diffraction (GIXRD, PANalytical Empyrean) and X-ray photoelectron spectroscopy (XPS, ESCALAB 250), respectively. The temperature-dependent and magnetic-field dependent resistances were measured by a physical property measurement system (Cryogenic CFMS-14T) using the four-probe method. The magnetic field was applied

perpendicular to the sample.

Results and Discussion

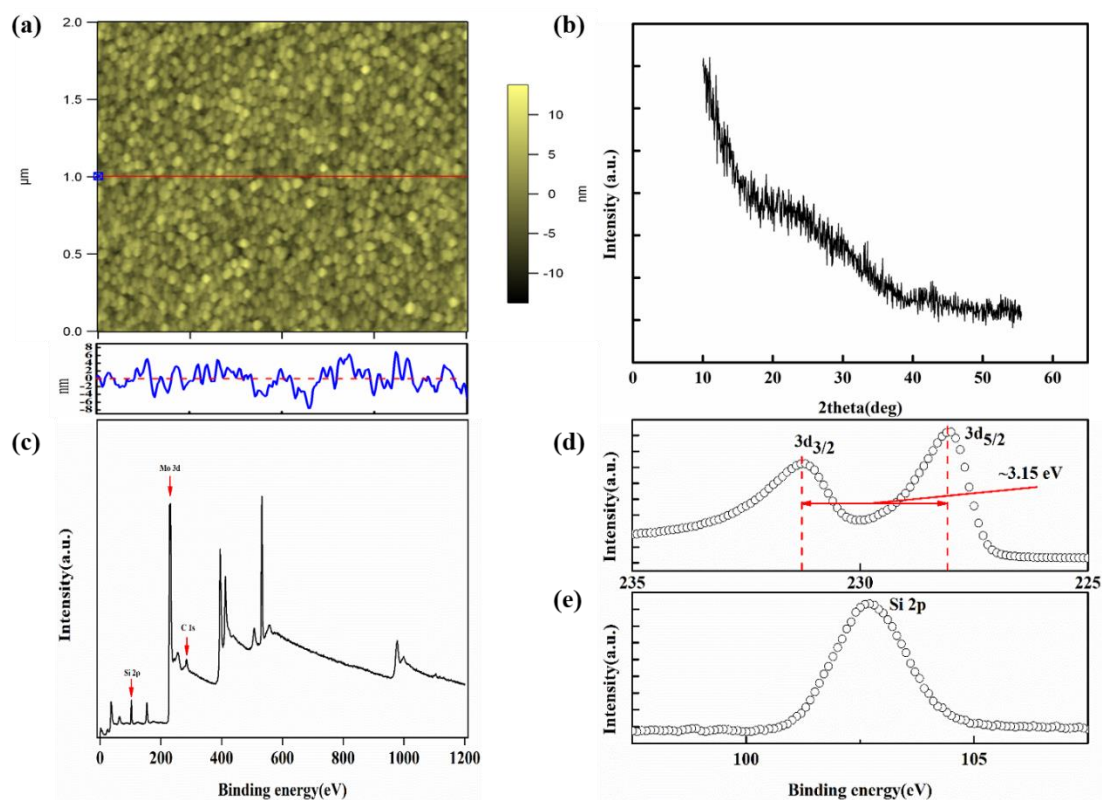


Figure 1 Morphology, structure and composition characterization of *a*-MoSi thin film. (a) AFM topographical image and the corresponding cross-section profile, (b) GIXRD pattern, (c) XPS full spectrum, (d) high-resolution Mo 3d spectrum, (e) high-resolution Si 2p spectrum.

Figure 1 (a) shows the surface morphology and the corresponding cross-section profile of *a*-MoSi thin film, demonstrating the uniform crack-free microstructure with root-mean-square surface roughness of 4.2 ± 0.1 nm. No typical diffraction peaks in the GIXRD pattern of *a*-MoSi thin film, as shown in Figure 1 (b), evidencing the amorphous phase of this sample. Figure 1 (c) depicts the XPS full spectrum of *a*-MoSi thin film, indicating the existence of Mo and Si elements, as marked by the red arrow. Furthermore, high-resolution XPS results of Mo 3d and Si 2p are given in

Figure 1 (d) and (e), respectively. Two distinct peaks centered at ~ 228 eV and ~ 231 eV, corresponding to $3d_{5/2}$ and $3d_{3/2}$, respectively, are observed in Mo $3d$ XPS spectrum (Figure 1(d)), due to the spin-orbital coupling effect [23]. The binding energies and the corresponding spin-orbit splitting energy (~ 3.15 eV) in a -MoSi thin film are consistent with the previously reported data in the case of MoO₂ [24], implying the molybdenum ions with the chemical state Mo⁴⁺. As shown in Figure 1(e), the Si $2p$ XPS spectrum exhibits a high symmetric peak at ~ 103 eV, revealing the -4 valence state of silicon in the sample, as observed in other Si-based amorphous materials [25]. Additionally, from the XPS spectra of Si $2p$ and Mo $3d$, the chemical composition ratio of a -MoSi thin film is obtained to be around 1.00 ± 0.04 .

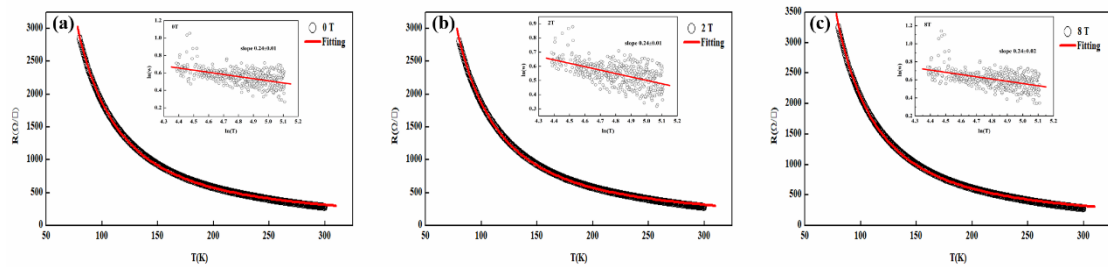


Figure 2 Temperature-dependent sheet resistance and the corresponding Zabrodskii analysis

(insets) at different magnetic field, (a) 0T, (b) 2T, (c) 8T. The red solid lines in figures show the fitting results.

Figure 2 depicts the temperature-dependence of sheet resistance under different magnetic field, demonstrating the semiconductor behaviors in the measured temperature region. The thermal activation model and the variable-range hopping (VRH) model were generally utilized to analyze the transport mechanism [26, 27]. Here, a self-consistent method, *i.e.*, Zabrodskii analysis [28], was used to specifically decide the transport mechanism. The logarithmic derivative

$w = -d(\ln(R))/d(\ln(T)) = p \cdot (T_0/T)^p$ is introduced, where T_0 is the characteristic parameter, T is the temperature, and p is the exponential term [29]. Different p values correspond to different conduction mechanisms, for example, the thermal activation model ($p=1$), the Mott-VRH model ($p=1/4$) [30], and the Efros-Shklovskii (ES) VRH model ($p=1/2$) [31]. As shown in the insets of Figure 2, $\ln(w)$ exhibits a linear relationship with $\ln(T)$, and all the slopes of $\sim 1/4$ were determined, indicating the Mott-VRH conduction mechanism in the α -MoSi thin film, as analogously reported in other amorphous binary compounds [21]. The α -MoSi thin film possesses disorder microstructure, as demonstrated above in GIXRD result, and thus the electronic wave-functions are localized, leading to the hopping of the charge carriers between adjacent or nearby localized states near the Fermi level.

Additionally, based on the Mott-VRH fitting results, as shown in Figure 2 (red solid lines), the characteristic parameter, T_0 , would be calculated to be 3.05×10^5 K (0T), 2.85×10^5 K (2T) and 3.73×10^5 K (8T) for the α -MoSi thin film. The T_0 decreases first and then increases as the magnetic field increases from 0T to 8T. According to the equation $T_0 = 18.1/(k_B g_0 a_0^3)$ (g_0 is the constant Mott density of states and a_0 is the localization length) [30], the trend of a_0 is opposite to that of T_0 . As the magnetic field rises, the localization length a_0 expands first and then shrinks, corresponding to the changes of volume of the localized state. Such trend of the localization length with magnetic field might be closely related to the interesting magneto-resistance (MR) behavior, as discussed below.

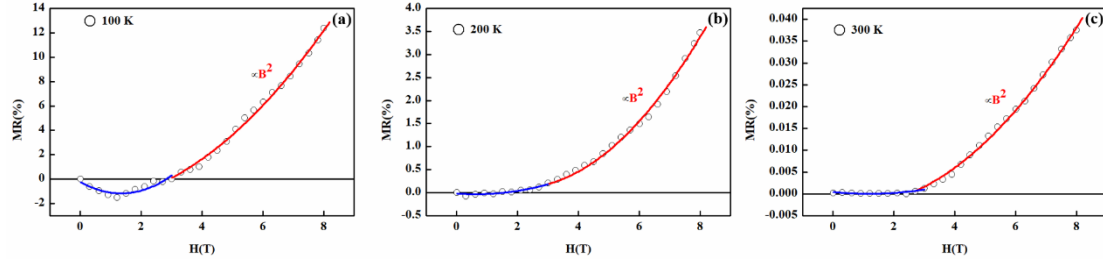


Figure 3 Magnetic-field dependence of MR in *a*-MoSi thin film at different temperatures, (a) 100 K, (b) 200 K, (c) 300 K.

Figure 3 presents the magnetic-field dependent magneto-resistance (MR) at different temperatures. Here, MR is defined as $MR = (R(H) - R(0)) / R(0) \times 100\%$, where $R(H)$ and $R(0)$ are the sheet resistance of *a*-MoSi thin film at magnetic field of H and zero, respectively. With increasing magnetic field, the crossover from negative to positive MR was observed at low temperature, *i.e.*, 100K. The negative MR characteristic, however, was weakened and disappeared at high temperature, *i.e.*, 300K. Similar phenomena were observed in some amorphous materials, for example, Ni_xSi_{1-x} [21]. For the hopping conduction regime in disorder materials, the probability of hopping at the two possible hopping sites can be easily varied under an applied magnetic field, leading to the MR.

To better understand the crossover from negative to positive MR, it is reasonably presumed that MR is the result of competition of positive MR (pMR) and negative MR (nMR):

$$MR = pMR + nMR$$

pMR is accepted to be related to the wave-function shrinkage effect [32, 33]. Under the strong magnetic field, the wave-function will be squeezed and the exponential tail of the wave-function will be less overlapped, resulting in the decreased hopping

probability between two sites and thus the increased resistance, *i.e.*, positive MR. Also, the relationship between pMR and magnetic field H can be expressed as $\text{pMR} \propto H^2$ [33]. As shown in Figure 3 (red solid lines), the fitting results are very consistent with the experimental data.

On the other hand, nMR is accepted to be associated with the electron wave-function interference effect [34]. As demonstrated above, the localization length, a_0 , increases with increasing magnetic field at the interval of 0-2 T, which may be due to the fact that the electron wave-function must increase its volume to find possible states with similar energies to achieve the charge transition [32]. When electrons hop between two possible sites, a larger a_0 indicates a stronger wave-function interference along random paths, and thus the hopping probability between two sites is increased and the resistance is decreased, *i.e.*, negative MR. Normally, the empirical equation [21], $\text{nMR} \propto -H$, can be used to describe the nMR caused by the interference effect. In our case, the low-field MR comprises of the contribution of the wave function shrinkage effect and the electron wave-function interference effect. As shown in Figure 3 (blue solid lines), the fitting curves match well with the experimental data. Moreover, it should be noted that this interference effect is more pronounced at lower temperature [32, 34]. This is why the nMR is more obvious at lower temperatures in our case. For example, at 100 K (see Figure 3(a)), pMR is mainly cancelled by nMR at low magnetic field, resulting in a whole negative MR. With increasing temperature, the interference effect is weakened, due to the enhanced jump probability between the two nearest neighbors, resulting in the reduced possible hopping paths between two

sites. Accordingly, the contribution of nMR is reduced and the positive MR will be over the negative MR at high temperature (see Figure 3(b) and (c)).

Conclusions

In summary, the amorphous molybdenum silicide thin film were grown on silicon substrates at room temperature by RF magnetron sputtering technique, and the charge transport behaviors were studied by measuring the temperature-dependent resistance and magneto-resistance data. The temperature-dependent resistance was analyzed through a self-consistent method, and the Mott-VRH transport mechanism causing by the disorder-induced electronic wave-function localization was confirmed. The crossover from negative to positive MR was observed with increasing magnetic field. The positive MR is primarily ascribed to the electron wave-function shrinkage effect, whereas the negative MR is mainly due to the electron wave-function interference effect.

Acknowledgements

This work was supported by the National Key Research and Development Program of China (2017YFB0503300) and the Fundamental Research Funds for the Central Universities (Nos. 310201911cx024, 310201911fz048).

References

- [1] B. Baeka, A.E. Lita, V. Verma, S.W. Nam, *Appl. Phys. Lett.* **98** (2011) 251105.
- [2] V.B. Verma, A.E. Lita, M.R. Vissers, F. Marsili, D.P. Pappas, P.R. Mirin, S.W. Nam, *Appl. Phys. Lett.* **105** (2014) 022602.
- [3] A. Banerjee, L.J. Baker, A. Doye, M. Nord, R.M. Heath, K. Erotokritou, D.

Bosworth, Z.H. Barber, I. MacLaren, R.H. Hadfield, *Supercond. Sci. Tech.* **30** (2017)

084010.

[4] M.M. Collver, R.H. Hammond, *Phys. Rev. Lett.* **30** (1973) 92.

[5] V.B. Verma, B. Korzh, F. Bussi ères, R.D. Horansky, S.D. Dyer, A.E. Lita, I.

Vayshenker, F. Marsili, M.D. Shaw, H. Zbinden, R.P. Mirin, S.W. Nam, *Opt. Express*

23 (2015) 33792.

[6] H.T. Huy, H. Shishido, M. Hayashi, T. Yotsuya, M. Kato, T. Ishida, *Physica C* **484**

(2013) 86.

[7] M.L. Liang, M.N. Kunchur, 2010 *Phys. Rev. B* **82** (2010) 144517.

[8] F. Colauto, M. Motta, A. Palau, M.G. Blamire, T.H. Johansen, W.A. Ortiz, *IEEE T.*

Appl. Supercond. **25** (2015) 1.

[9] M. Motta, F. Colauto, J.I. Vestg ården, J. Fritzsche, M. Timmermans, J. Cuppens, C.

Attanasio, C. Cirillo, C.C. Moshchalkov, J.V. Vondel, T.H. Johansen, W.A. Ortiz, A.V.

Silhanek, *Phys. Rev. B* **89** (2014) 134508.

[10] C.M. Natarajan, M.G. Tanner, R.H. Hadfield, *Supercond. Sci. Tech.* **25** (2012)

63001.

[11] Y.P. Korneeva, M.Y. Mikhailov, Y.P. Pershin, N.N. Manova, A.V. Divochiy, Y.B.

Vakhtomin, A.A. Korneev, K. V. Smirnov, A.G. Sivakov, A.Y. Devizenko, G.N.

Goltsman, *Supercond. Sci. Tech.* **27** (2014) 95012.

[12] M. Caloz, B. Korzh, N. Timoney, M. Weiss, S. Gariglio, R.J. Warburton, C.

Schönenberger, J. Renema, H. Zbinden, F. Bussi ères, *Appl. Phys. Lett.* **110** (2017)

083106.

- [13] H.B. Zhang, L. Xiao, B.C. Luo, J.H. Guo, L.B. Zhang, J. Xie, *J. Phys. D: Appl. Phys.* **53** (2020) 013001.
- [14] L. Ceccarelli, D. Vasyukov, M. Wyss, G. Romagnoli, N. Rossi, L. Moser, M. Poggio, *Phys. Rev. B* **100** (2019) 104504.
- [15] G. Grimaldi, A. Leo, P. Sabatino, G. Carapella, A. Nigro, S. Pace, V.V. Moshchalkov, A.V. Silhanek, *Phys. Rev. B* **92** (2015) 024513.
- [16] A. Leo, G. Grimaldi, A. Nigro, E. Bruno, F. Priolo, S. Pace, *Physica C* **503** (2014) 140.
- [17] N. Kokubo, H. Tamochi, B. Shinozaki, T. Nishizaki, N. Kobayashi, *J. Phys. Conf. Ser.* **400** (2012) 022057.
- [18] S. Okuma, D. Shimamoto, N. Kokubo, *Phys. Rev. B* **85** (2012) 064508.
- [19] S. Ikeda, K. Miura, H. Yamamoto, K. Mizunuma, H.D. Gan, M. Endo, S. Kanai, J. Hayakawa, F. Matsukura, H. Ohno, *Nat. Mater.* **9** (2010) 721.
- [20] H. Mell, J. Stuke, *J. Non-cryst. solids* **4** (1970) 304.
- [21] R. Rosenbaum, T. Murphy, E. Palm, S. Hannahs, B. Brandt, *Phys. Rev. B* **63** (2001) 094426.
- [22] S. Yoshizumi, T. H. Geballe, M. Kunchur, W.L. McLean, *Phys. Rev. B* **37** (1988) 7094.
- [23] Christopher J. Foot, *Atomic Physics*, 1st ed., Oxford University Press, Oxford, 2005.
- [24] J. G. Choi, L.T. Thompson, *Appl. Surf. Sci.* **93** (1996) 143.
- [25] Akihiro Kitao, Kenji Imakita, Ibuki Kawamura, Minoru Fujii, *J. Phys. D: Appl.*

Phys. **47** (2014) 215101.

[26] S.K. Sharma, R.K. Shukla, A. Kumar, Physica B **481** (2016) 144.

[27] Deepika, H. Singh, Can. J. Phys. **97** (2019) 222.

[28] A.G. Zabrodskii, Philos. Mag. B **81** (2001) 1131.

[29] B.C. Luo, J.B. Hu, ACS Appl. Electron. Mater. **1** (2019) 51.

[30] N.F. Mott, J. Non-cryst. solids **1** (1968) 1.

[31] A.L. Efros, B.I. Shklovskii, J. Phys. C: Solid State Phys. **8** (1975) L49.

[32] W. Schoepe, Physik B - Condensed Matter **71** (1988) 455.

[33] B.I. Shklovskii, A.L. Efros, Electronic Properties of Doped Semicondors, 1st ed., Springer, Dordrecht, 1984.

[34] V.L. Nguyen, B.Z. Spivak, B.I. Shklovskii, J. Exp. Theoretical Phys. **62** (1985) 1021.